Fermi-surface anomaly for neutrons in yttrium

C. Mahaux and R. Sartor
Institut de Physique B5, Université de Liège, Sart Tilman, B-4000 Liège 1, Belgium
(Received 17 June 1987)

The dispersion relation approach is used to extrapolate towards negative energy the average potential felt by neutrons in yttrium, using as input empirical values of the optical-model potential. At positive energy the absolute value of the volume integral of the potential decreases approximately linearly with energy, but it sharply increases with energy in the vicinity of the Fermi energy, i.e., in the domain which corresponds to the valence bound neutron shells. This Fermi-surface anomaly is quite similar to that which has recently been investigated in the case of neutrons in ^{208}Pb. It mainly reflects the energy dependence of the potential radius, although the energy dependence of the potential depth also has a characteristic nonmonotonic behavior and plays a significant role. The energy and radial dependence of the effective mass is exhibited.

I. INTRODUCTION

Optical-model analyses of scattering cross sections show that, at positive energy, the average nucleon-nucleus potential depends upon energy. In contrast, the experimental single-particle energies of the valence shells, which are negative, can be reproduced with an average potential which is independent of energy. This modification of the energy dependence of the average potential as the energy changes sign is often called "the Fermi-surface anomaly."

Its existence[1] as well as its physical origin[2] were pointed out long ago, but is is only recently that the detailed nature of the energy dependence of the average potential near the Fermi energy has been exhibited;[3] is was found to be quite similar in ^{40}Ca as in ^{208}Pb. The theory, furthermore, makes one expect that it should also be approximately the same for the other medium-weight and heavy nuclei.

This expectation appears to be at variance with a recent analysis[4] from which it is concluded that "the neutron interaction with ^{89}Y does not display a Fermi-surface anomaly of the nature reported in the ^{208}Pb region" in Ref. 3. The main purpose of the present work is to perform an improved analysis of the n-^{89}Y system in the framework of the dispersion relation approach outlined in Ref. 5 and discussed in detail in Refs. 6 and 7. This will lead us to the conclusion that the Fermi-surface anomaly is quite similar in the n-^{89}Y as in the n-^{208}Pb system. In particular, the potential radius increases and the potential depth decreases with energy in the vicinity of the Fermi surface, while at positive energy the potential radius and the potential depth both decrease with energy. These main features are expected to be shared by all nuclei.

Our presentation scheme is the following: In Sec. II we first briefly recall the dispersion relation approach of Refs. 5 and 6 and we specify the inputs of our analysis, namely the real and imaginary parts of empirical optical-model potentials for the n-^{89}Y system and the experimental single-particle energies. The Woods-Saxon parametrization of the real part of the average potential in the energy domain $-20 \leq E \leq 40$ MeV is calculated in Sec. III; we consider, in particular, the potential depth and radius, the volume integral per nucleon, the root mean square radius, and the effective mass. The main difference between the present analysis and the one carried out in Ref. 4 is discussed in Sec. IV. Our conclusions are presented in Sec. V.

II. EMPIRICAL INPUT

Let $M(r;E)=V(r;E)+iW(r;E)$ denote the nucleon-nucleus mean field. Our aim is to determine the radial and energy dependence of $V(r;E)$ at negative as well as at positive energy. We assume that $V(r;E)$ has a Woods-Saxon shape:

$$V(r;E)=-U_V f(x_V) , \tag{2.1a}$$

$$f(X_V)=\{1+\exp[(r-R_V)/a_V]\}^{-1} . \tag{2.1b}$$

The problem then amounts to finding the energy dependence of three parameters, namely $U_V(E)$, $R_V(E)$, and $a_V(E)$. Equivalently, it is sufficient to determine three different radial moments

$$[r^q]_V(E)=\frac{4\pi}{A}\int_0^\infty V(r;E)r^q dr . \tag{2.2}$$

This is possible in the framework of the dispersion relation approach of Refs. 5 and 6, which is briefly recalled in Sec. II A. The inputs of the calculation are the empirical values of the radial moments of the imaginary and real parts of the optical-model potential and the single-particle energies. These inputs are specified in Sec. II B.

A. Dispersion relation approach

In this approach $V(r;E)$ is written as the sum of the Hartree-Fock– (HF-) type component $V_{\rm HF}(r;E)$ and of a dispersive contribution $\Delta V(r;E)$:

$$V(r;E)=V_{\rm HF}(r;E)+\Delta V(r;E) , \tag{2.3}$$

$$[r^q]_V(E)=[r^q]_{\rm HF}(E)+[r^q]_{\Delta V}(E) \ . \tag{2.4}$$

We shall determine $[r^q]_{\Delta V}(E)$ from the following dispersion relation,

$$[r^q]_{\Delta V}(E)=\frac{P}{\pi}\int_{-\infty}^{\infty}\frac{[r^q]_W(E')}{E'-E}dE' \ ; \tag{2.5}$$

P denotes a principal value. It is plausible to assume that $[r^q]_W(E')$ is symmetric with respect to the Fermi energy E_F since this amounts to assuming that for a given excitation energy $|E'-E_F|$ the absorptive potential is approximately the same in the $(A+1)$ as in the $(A-1)$ nucleus.[3,8,9] Equation (2.5) can then be written in the form

$$[r^q]_{\Delta V}(E)=\frac{2}{\pi}(E_F-E)P\int_0^{\infty}\frac{[r^q]_W(E'+E_F)}{(E-E_F)^2-E'^2}dE' \ . \tag{2.6}$$

The moments $[r^q]_{\Delta V}(E)$ can thus be determined from the empirical energy dependence of $[r^q]_W(E)$ as derived from phenomenological optical-model potentials; algebraic parametrizations of $[r^q]_W(E)$ will be constructed in Sec. II B.

The problem then amounts to determine the radial moments of the Hartree-Fock–type component. These are expected to be smooth monotonic functions of energy. We shall approximate them by linear expressions

$$[r^q]_{\rm HF}(E)=A_q+B_qE \ . \tag{2.7}$$

The coefficients A_q,B_q will be determined by least squares fits to the empirical values $[r^q]_V(E_k)$ of the real parts of empirical optical-model potential; E_k denotes an energy at which an optical-model analysis has been performed. The values of $[r^q]_V(E_k)$ will be specified in Sec. II C.

Once this is performed the values of $[r^q]_V(E)$ are known over the entire range of energies in which the approximations are justified. Here we shall mostly limit ourselves to the domain $-20<E<40$ MeV. From three different values of $[r^q]_V(E)$, for instance[5,6] from $[r^{0.8}]_V(E)$, $[r^2]_V(E)$, and $[r^4]_V(E)$, one can determine the three Woods-Saxon parameters $U_V(E)$, $R_V(E)$, and $a_V(E)$. These will be considered zeroth order approximations and will be improved by iteration, as we now outline.

The accuracy of the approach can be checked by calculating the energies of the bound single-particle states and comparing them with the experimental values E_{nlj}; some typical spin-orbit potential must, of course, be introduced. The resulting agreement is fair. It can be improved as follows.[5,6] One considers the radial moments determined as above as zeroth order approximations, say $[r^q]_V^{(0)}(E)$. With the corresponding geometrical parameters $R_V^{(0)}(E_{nlj})$, $a_V^{(0)}(E_{nlj})$, and some typical spin-orbit potential, we determine the depths $U_V^{(1)}(E_{nlj})$ which reproduce the experimental single-particle energies $E_{nlj}<0$. The set $\{R_V^{(0)}(E_{nlj}), a_V^{(0)}(E_{nlj}), U_V^{(1)}(E_{nlj})\}$ enables one to determine first order approximations, say $[r^q]_V^{(1)}(E_{nlj})$, to the radial moments. By least squares fits to the empirical values $\{[r^q]_V^{(1)}(E_{nlj}), [r^q]_V(E_k)\}$, one determines new values, say $A_q^{(1)},B_q^{(1)}$, of the coefficients of the linear approximation to $[r^q]_{\rm HF}(E)$. Note that the fits now take into account the radial moments $[r^q]_V^{(1)}(E_{nlj})$ at the *negative* energies E_{nlj}. The procedure can be repeated until the coefficients A_q,B_q remain unchanged under iteration. In practice, one or at most two iterations are sufficient.

As discussed in Ref. 6, the calculated values of a_V are quite sensitive to small changes of the input empirical values $[r^q]_V(E_k)$. It is therefore not possible to determine reliably the energy dependence of a_V. Hence we use here a simplified version[6] of the dispersion relation approach in which one keeps a_V fixed at an average empirical value. We take[4]

$$a_V=0.70 \text{ fm} \ . \tag{2.8}$$

Only two Woods-Saxon parameters, namely U_V,R_V, then remain to be determined. We shall calculate them by applying the dispersion relation approach to the radial moments $[r^{0.8}]_V$ and $[r^2]_V$. As a check of the consistency of the calculation, we shall compare the calculated $[r^4]_V(E)$ with the empirical values. Correspondingly, we shall compare with empirical evidence the calculated values of the mean square radius $[r^4]_V/[r^2]_V$.

In the present work we adopt, in part, the same empirical inputs as in Ref. 4, with important additions that we discuss in Sec. IV. In particular, we take the same spin-orbit coupling as Lawson *et al.*,[4] namely

$$V_{ls}=U_{ls}r^{-1}\frac{d}{dr}f(X_{ls})\boldsymbol{l}\cdot\boldsymbol{\sigma} \ , \tag{2.9a}$$

with

$$U_{ls}=11.5 \text{ MeV}, \quad r_{ls}=1.025 \text{ fm}, \quad a_{ls}=0.40 \text{ fm} \ . \tag{2.9b}$$

B. Empirical optical-model potentials and single-particle energies

Accurate measurements of differential-elastic n-^{89}Y cross sections between 4 and 10 MeV are reported in Ref. 4. Very good optical-model fits were obtained, taking for $W(r;E)$ a surface-peaked form:

$$W_d(r;E)=4W_d^{(0)}(E)a_d\frac{d}{dr}f(X_d) \ , \tag{2.10}$$

with $(4.5\le E\le 10$ MeV)

$$a_d=(0.1661+0.0284E) \text{ fm} \ , \tag{2.11a}$$

$$r_d=(1.5336-0.0255E) \text{ fm} \ . \tag{2.11b}$$

The values of the volume integral per nucleon $[r^2]_W$ plotted in Fig. 2 of Ref. 4 determine the corresponding strength $W_d^{(0)}(E_k)$. In addition, that figure also provides the value of $W_d^{(0)}$ at 2.75 MeV, as determined from fitting simultaneously several differential cross sections for energies between 1.5 and 4.0 MeV, at approximately 50 keV intervals. This enables one to determine the values of $[r^{0.8}]_W(E)$ and $[r^2]_W(E)$ represented by the

crosses located at 2.75, 4.5, 5.0, 5.5, 5.9, 6.5, 7.1, 7.5, 8.03, 8.40, 9.05, 9.5, and 10.0 MeV in Fig. 1.

For energies larger than 10 MeV, we follow the authors of Ref. 4 and adopt the optical-model potential of Walter and Guss,[10] with the following important difference. Walter and Guss[10] write the absorptive potential as the sum of a Woods-Saxon shape and of a surface-peaked contribution,

$$W(r;E)=W_v(r;E)+W_d(r;E)\ , \tag{2.12}$$

where $W_v(r;E)$ is different from zero. In their analysis, Lawson *et al.*[4] omit the volume absorption $W_v(r;E)$ and only retain $W_d(r;E)$. As discussed in Sec. IV, this is not justified. Here we retain both $W_v(r;E)$ and $W_d(r;E)$; we calculate the corresponding values of $[r^{0.8}]_W(E)$ and $[r^2]_W(E)$. They are represented by the crosses located at 15, 20, 25, 30, 35, and 40 MeV in Fig. 1.

The solid curves in Fig. 1 represent least squares fits to the empirical values (crosses) with the following parametric form proposed by Brown and Rho (Br),[11]

$$[r^q]_W^{\rm BR}(E)=-b_q\frac{(E-E_F)^2}{(E-E_F)^2+r_q^2}\ . \tag{2.13}$$

The Fermi energy E_F lies halfway between the occupied and unoccupied valence shells. We adopt the same value as in Ref. 4, namely

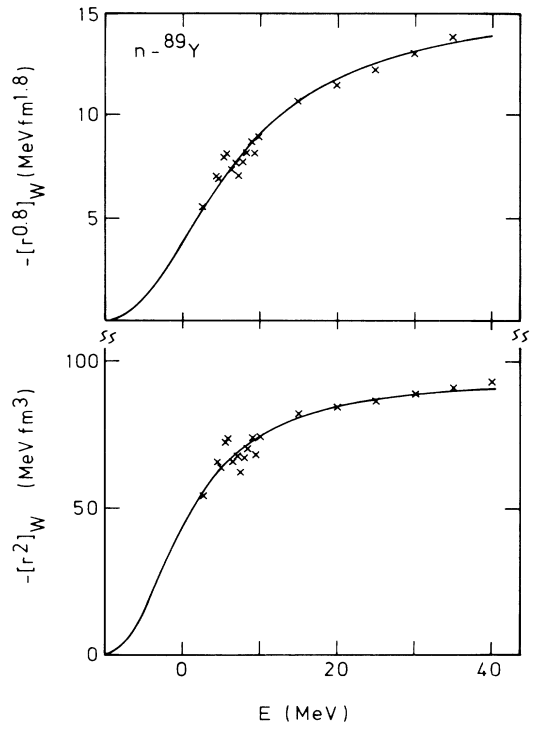

FIG. 1. Energy dependence of the radial moments $[r^{0.8}]_W$,$[r^2]_W$ of the imaginary part of the mean field for the n-^{89}Y system. The crosses are empirical values (Sec. II B) and the curves represent least squares fits with the Brown-Rho parametrization, Eq. (2.13).

TABLE I. Parameters of the least squares fits to $[r^q]_W$ and $[r^q]_V$.

q	b_q (MeV fm^{q+1})	r_q (MeV)	A_q (MeV fm^{q+1})	B_q (fm^{q+1})
0.8	15.4	15.9	−79.54	0.50
2	93.6	9.78	−415	2.64

$$E_F=-9.1\ \text{MeV}\ . \tag{2.14}$$

The values of the parameters b_q and r_q are listed in Table I. The Brown-Rho parametrization presents the interest of yielding an algebraic expression for the radial moments of the dispersive contribution, viz. ($r_q>0$),

$$[r^q]_{\Delta V}^{\rm BR}(E)=-b_q r_q\frac{E-E_F}{(E-E_F)^2+r_q^2}\ . \tag{2.15}$$

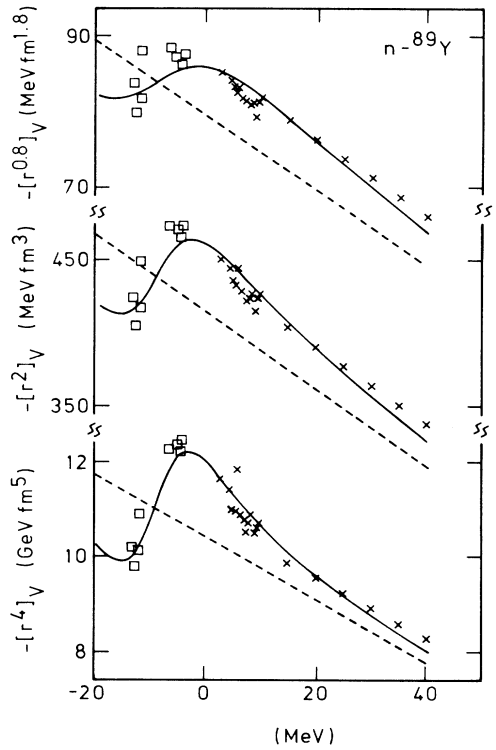

FIG. 2. Energy dependence of the radial moments of the real part of the mean field for the n-^{89}Y system. The crosses are obtained from empirical optical-model potentials, as specified in Sec. II B. The squares are located at the experimental single-particle energies and are calculated from Woods-Saxon potentials with diffuseness $a_V=0.70$ fm and with a radius represented by the solid curve in the middle of Fig. 3. The solid curves for $[r^{0.8}]_V$ and $[r^2]_V$ are least squares fits performed in the framework of the dispersion relation approach (Sec. II A). In the case of $[r^4]_V(E)$ the solid curve is predicted from the Woods-Saxon parameters represented by the solid curves in Fig. 3. The dashed curves represent the linear energy dependence of the Hartree-Fock–type contribution.

We now turn to the radial moments of the real parts of the empirical optical-model potentials. For $E_k \leq 10$ MeV we compute them from the potentials obtained in Ref. 4. There, $R_V = r_V A^{1/3}$ was assumed to be constant ($r_V = 1.24$ fm), while the values of $a_V(E_k)$ and of the volume integral per nucleon $[r^2]_V(E_k)$ are plotted in Fig. 1 of Ref. 4. This information is sufficient to obtain U_V and, thereby, the values of $[r^q]_V(E_k)$. The resulting values of the radial moments are represented by the crosses located at $E_k = 2.75$, 4.5, 5.0, 5.5, 5.9, 6.5, 7.1, 7.5, 8.03, 8.40, 9.05, 9.5, and 10.0 MeV in Fig. 2. The crosses located at 15, 20, 25, 30, 35, and 40 MeV are obtained from the global empirical optical-model potential of Walter and Guss.[10]

The last input needed for applying the dispersion relation approach is a set of experimental single-particle energies; for these we adopted the same values as Lawson *et al.*[4] They were deduced from the energies of single-particle states ($1f_{5/2}$, $2p_{3/2}$, $2p_{1/2}$, $1g_{9/2}$, $2d_{5/2}$, $3s_{1/2}$, $2d_{3/2}$, and $1g_{7/2}$) in ^{88}Sr, with corrections due to the difference of radius and neutron excess between ^{89}Y and ^{88}Sr. In view of these corrections, the accuracy of these single-particle energies is probably not better than a few hundreds of keV.

III. EXTRAPOLATION OF THE WOODS-SAXON PARAMETRIZATION OF $V(r;E)$

A. Woods-Saxon parameters

We now carry out the dispersion relation analysis of the radial moments $[r^{0.8}]_V$,$[r^2]_V$ as outlined in Sec. II A. Only two radial moments are involved since we set the diffuseness equal to 0.70 fm; this only leaves two unknowns in the Woods-Saxon parametrization, namely the depth U_V and the radius parameter $r_V = R_V A^{-1/3}$. As in the case n-^{208}Pb,[6] only two iterations are sufficient to ensure convergence. The resulting values of $[r^{0.8}]_V(E)$ and $[r^2]_V(E)$ are represented by the solid curves in the upper part of Fig. 2, while the Woods-Saxon parameters are plotted in Fig. 3.

The solid curves closely follow the energy dependence delineated by the empirical crosses and squares. This agreement is satisfactory, especially if one takes into account the fact that the open squares are related to single-particle energies extrapolated from ^{88}Sr, and that any mean field model can only describe the average energy dependence since it does not explicitly include the coupling to specific core excitations. An additional check of the reliability of our approach is provided by the moment $[r^4]_V$. From the values of $U_V(E)$, $r_V(E)$, and a_V plotted in Fig. 3, one can indeed predict the value of $[r^4]_V(E)$; it is represented by the solid curve at the bottom of Fig. 2. The good agreement between this prediction and the empirical points confirms the accuracy of our method.

The straight dashed curves in the upper drawings of Fig. 2 represent the Hartree-Fock–type contribution to the radial moments $[r^{0.8}]_V$ and $[r^2]_V$, Eq. (2.7). If one makes the assumption that $V_{HF}(r;E)$ has a Woods-Saxon shape with diffuseness $a_{HF} = 0.70$ fm, $[r^{0.8}]_{HF}(E)$ and $[r^2]_{HF}(E)$ yield the Woods-Saxon parameters represented by the dashed lines in Fig. 3. In turn, these yield the moment $[r^4]_{HF}(E)$ plotted at the bottom of Fig. 2; it is approximately a straight line, which confirms the consistency of our assumptions.

Our results are quite similar to those recently found in the case of neutrons in ^{208}Pb,[5,6,12] in particular the following:

(i) In the vicinity of the Fermi energy, the potential depth is approximately the same for the full potential as for its Hartree-Fock–type component.

(ii) For $E - E_F > 20$ MeV the depth of the full potential is approximately 5 MeV larger than that of its Hartree-Fock component, but it has approximately the same energy derivative.

(iii) The potential depth is approximately independent of energy for $0 < E < 10$ MeV.

(iv) The potential radius sharply increases with energy

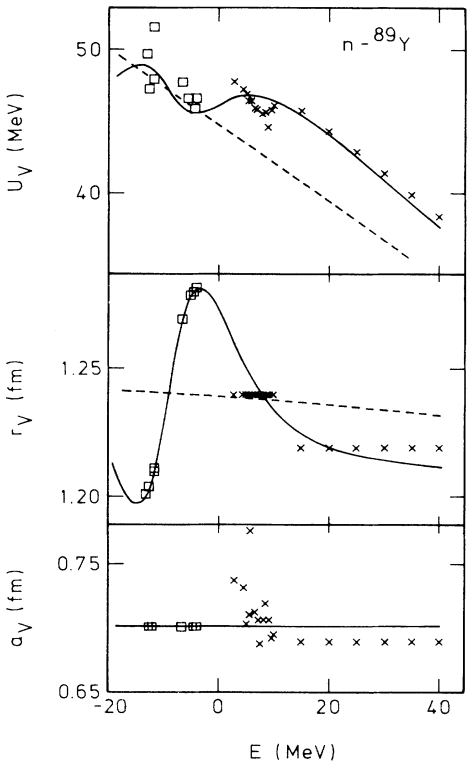

FIG. 3. Energy dependence of the Woods-Saxon parameters. The solid curves represent the depth $U_V(E)$ and the radius parameter $r_V(E)$ deduced from the radial moments $[r^{0.8}]_V(E)$,$[r^2]_V(E)$ plotted in Fig. 2; the diffuseness a_V has been set equal to 0.70 fm. The crosses are empirical values associated with the optical-model potentials of Ref. 4 (for $2.75 \leq E_k \leq 10$ MeV) and Ref. 10 (for $E_k \geq 15$ MeV). The squares are located at the experimental single-particle energies; by construction they lie on the solid curves in the case of the geometrical parameters r_V,a_V; the associated depths are calculated in such a way that the Woods-Saxon potential has a bound state at the corresponding single-particle energy, using the spin-orbit potential specified by Eqs. (2.9a) and (2.9b).

in the vicinity of the Fermi energy ($|E-E_F|<5$ MeV), but decreases with energy for $E-E_F \gtrsim 10$ MeV.

(v) The increase of $[r^q]_V(E)$ for E close to E_F is due to the increase of the potential radius.

(vi) At the Fermi energy, the radius parameter r_V is equal to 1.24 fm. This is the same value as that determined for the n-^{208}Pb system in Ref. 12, where a_V was taken equal to 0.68 fm; in Ref. 6 the calculated value of $r_V(E_F)$ for n-^{208}Pb is approximately equal to 1.27 fm (for $a_V=0.70$ fm), but is somewhat inaccurate because of the poor knowledge of the empirical optical-model potentials for energies larger than 25 MeV.

B. Dispersive contribution

From the Woods-Saxon parameters plotted in Fig. 3 one can obtain the potential $V(r;E)$, its Hartree-Fock contribution $V_{\rm HF}(r;E)$, and their difference $\Delta V(r;E)=V(r;E)-V_{\rm HF}(r;E)$. These quantities are represented in Fig. 4, at the energies $E-E_F=5$ and 10 MeV. We recall that $\Delta V(r;E)$ vanishes at $E=E_F$.

At $E-E_F=5$ MeV, i.e., at $E=-4.1$ MeV, $\Delta V(r;E)$ has a surface-peaked shape, with diffuseness 0.70 fm. This is expected from the difference between two Woods-Saxon potentials with approximately the same depth and slightly different radii. The physical origin of this surface peaking is the same as that of the surface peaking of $W(r;E')$ for small E', namely the fact that at small energy the single-particle degree of freedom is mainly coupled to surface excitations of the core. We note that at $E-E_F=10$ MeV ($E=0.9$ MeV) the dispersive contribution $\Delta V(r;E)$ has a sizable volume component, although at that energy $W(r;E)$ is located at the surface, Eq. (2.10). This reflects the fact that $\Delta V(r;E)$ is expressed as a principal value integral which involves $W(r;E')$ for all E'. We return to this point in Sec. IV.

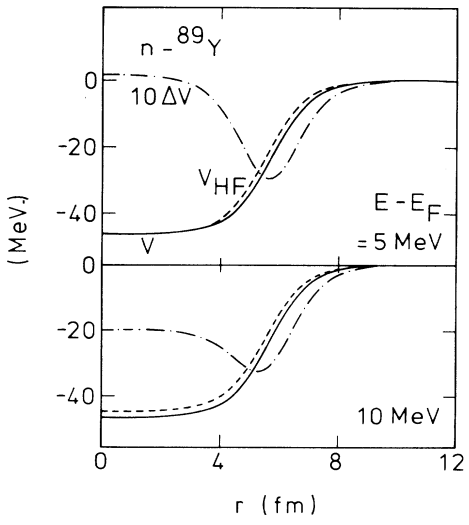

FIG. 4. Radial dependence of the full potential (solid curve), of its Hartree-Fock–type component (dashed curve), and of the dispersive contribution (multiplied by 10, dashed-dotted line), for $E-E_F=5$ MeV (top) and 10 MeV (bottom).

C. Ratios of radial moments

In the phenomenological analysis of Ref. 4 the radius parameter r_V was assumed to be constant in the energy domain $2.75 \le E \le 10$ MeV, while the diffuseness a_V was adjusted at each energy. In the present analysis, we have instead set a_V equal to a constant and have calculated an energy-dependent radius parameter; our motivation for doing so is that r_V is expected to be energy dependent on rather general grounds.[3,5,12] In view of this difference between the values of r_V, a_V adopted here and in Ref. 4, it is useful to characterize the range of the potential by its root mean square radius. We use the notation[13]

$$\langle r^2\rangle_V^{1/2}(E)=T_{4/2}(E)\ , \tag{3.1}$$

where

$$T_{q/q'}=\{[r^q]_V(E)/[r^{q'}]_V(E)\}^{1/(q-q')}\ . \tag{3.2}$$

Note that if any of the quantity $T_{q/q'}$ depends on energy, this implies that the radial shape of the potential varies with energy.[13]

The quantities $T_{2/0.8}$ and $T_{4/2}$ are plotted in Fig. 5.

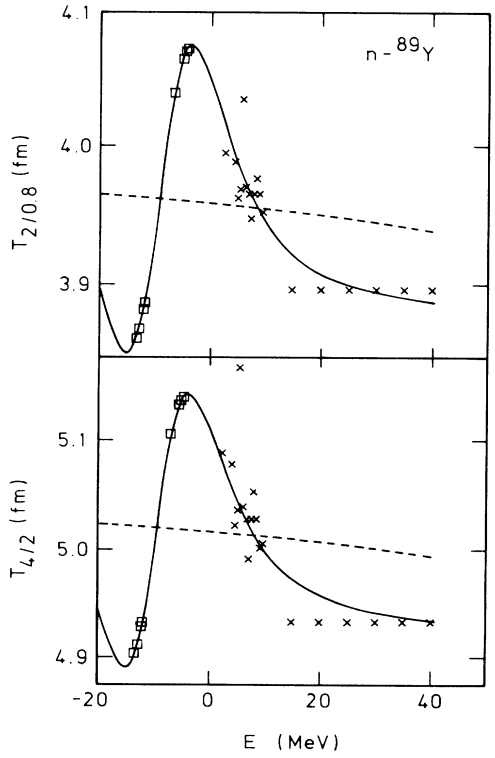

FIG. 5. Energy dependence of the moment ratios $T_{2/0.8}$ and $T_{4/2}$, Eq. (3.2). The crosses are empirical values derived from phenomenological optical-model potentials (Refs. 4 and 10). The solid curves are predictions of our dispersion relation approach; the dashed curves correspond to the Hartree-Fock–type contribution. The squares are located at the single-particle energies and lie on the solid curves, by construction.

The radial shape of the Hartree-Fock component is very approximately independent of energy. In contrast, the calculated moment ratios strongly increase with energy in the domain of the bound valence shells, while they decrease with energy at positive energy. The latter prediction is seen to be in close agreement with the empirical behavior. Empirical evidence for a decrease of $T_{4/2}$ and $T_{2/0.8}$ with increasing incident energy exists in other nuclei as well.[13]

D. Effective mass

The Fermi-surface anomaly consists of a nonmonotonic energy dependence of the potential parameters as the nucleon energy approaches E_F. Hence it has first been formulated[1] in terms of the derivative of the potential with respect to energy, which is conveniently characterized by the effective mass m^*. In a nucleus, the latter is defined by the relation

$$\frac{m^*(r;E)}{m}=1-\frac{d}{dE}V(r;E)\ . \tag{3.3}$$

It depends on the radial distance and energy.

If the dispersive contribution is neglected, the effective mass reduces to the Hartree-Fock–type contribution, namely

$$m^*_{\rm HF}(r;E)/m=1-\frac{d}{dE}V_{\rm HF}(r;E)\ . \tag{3.4}$$

This quantity is practically independent of energy. Its radial dependence at $E=E_F$ is represented by the dashed line in Fig. 6. It approximately has a Woods-Saxon shape, with $m^*_{\rm HF}(r=0;E_F)/m=0.73$. In contrast, the full effective mass $m^*(r;E_F)/m$ at the Fermi energy has a strong peak near the nuclear surface. This peak reflects the energy dependence of the radius parameter $r_V(E)$ for E close to E_F. It rapidly disappears as E becomes different from E_F.

The upper part of Fig. 7 represents the energy dependence of the surface value of the effective mass, namely of $m^*(r=5.54$ fm;$E)$. This quantity has a sharp maximum centered at the Fermi energy, with a full width at half maximum approximately equal to 10 MeV. The lower part of Fig. 7 shows the energy dependence of the central value of the effective mass, namely of $m^*(r=0;E)/m$. This quantity has maxima on both sides of E_F, namely at $|E-E_F|\approx 10$ MeV.

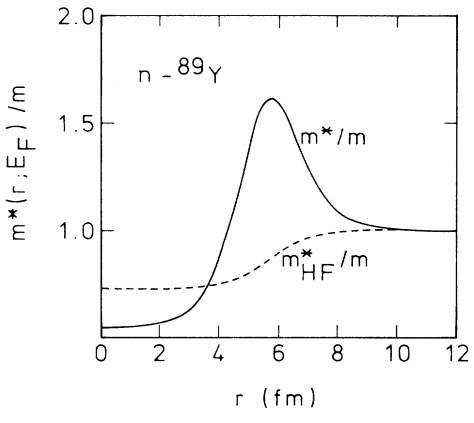

FIG. 6. Radial dependence of the effective mass $m^*(r;E_F)/m$ (solid curve) and of its Hartree-Fock–type component $m^*_{\rm HF}(r;E_F)/m$ (dashed curve) at the Fermi energy.

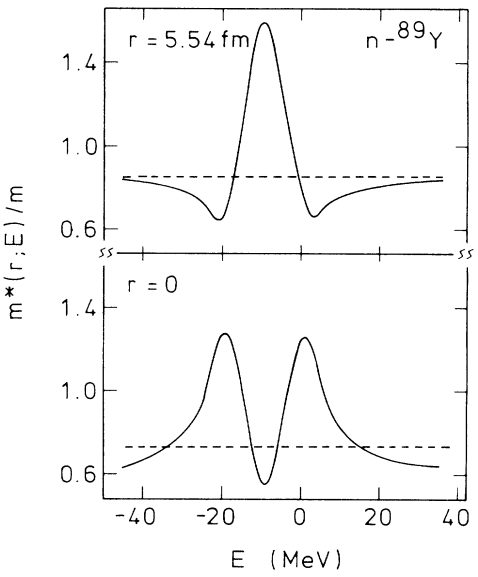

FIG. 7. Energy dependence of the effective mass (solid curves) and of its Hartree-Fock–type approximation (dashed lines) at the potential surface ($r=5.54$ fm, upper part) and at the nuclear center ($r=0$ fm, lower part).

IV. COMPARISON WITH A PREVIOUS ANALYSIS

All the properties found in Sec. III are very similar to those obtained in the case of neutrons on ^{208}Pb.[7,12] This indicates that the Fermi-surface anomaly is of the same nature in ^{89}Y as in ^{208}Pb. This conclusion differs from that drawn from a recent analysis of the n-^{89}Y system.[4] In this section we discuss the main differences between that analysis and the present one.

The dispersion relation (2.5) between the radial moments $[r^q]_{\Delta V}(E)$ and $[r^q]_W(E')$ is an integral form of the radial-dependent relation

$$\Delta V(r;E)=\frac{P}{\pi}\int_{-\infty}^{\infty}\frac{W(r;E')}{E'-E}dE'\ . \tag{4.1}$$

The following two main approximations have been made in Ref. 4:

(i) When applying the dispersion relation (2.5), the authors set $[r^2]_W(E')$ equal to zero for $E'<-18.2$ MeV. This amounts to assuming that the single-particle excitations of ^{88}Y have an infinite lifetime for excitation energies larger than 6.5 MeV. It is physically much more plausible to assume that the radial moment $[r^q]_W(E')$ is approximately symmetric with respect to E_F, as we do here and as recently adopted by Lawson *et al.*[14] in an analysis of the n-^{209}Bi system. This symmetry is sup-

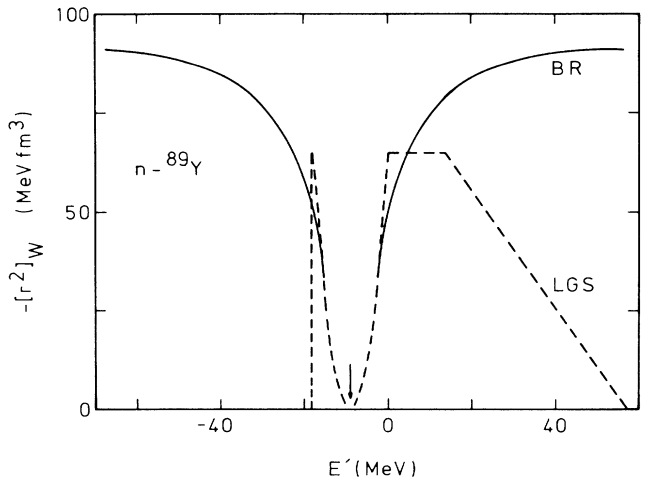

FIG. 8. Dependence on E' of the volume integral per nucleon of the imaginary part of the mean field, $[r^2]_W(E')$, which appears in the integrand of the dispersion relation (2.5) for $q=2$. The solid curve represents the input used here and specified in Sec. II B. The dashed line shows the values adopted in Ref. 4.

ported by microscopic calculations, as shown by, e.g., Fig. 4.45e of Ref. 8, as well as by empirical evidence (Fig. 4.6 of Ref. 8). It amounts to the property that single-particle excitations have approximately the same lifetime in ^{88}Y as in ^{90}Y for the same excitation energy (the fact that these two nuclei are unstable is irrelevant). The difference between the volume integrals $[r^2]_W(E')$ used in the present work and in Ref. 4 is illustrated in Fig. 8. The difference between the solid and the dashed curve in the domain $E'>20$ MeV is due to the fact that the authors of Ref. 4 omitted the contribution of the volume absorption in the global optical-model potential of Walter and Guss.[10]

(ii) The dispersive contribution $\Delta V(r;E)$ has been assumed to be entirely located at the nuclear surface; furthermore, its radial shape has been assumed to be the same as that of the absorptive potential $W(r;E)$ at the same energy E. This is not justified because $\Delta V(r;E)$ involves $W(r;E')$ for all E'. In particular, the value $\Delta V(r=0;E)$ of the dispersive contribution at the nuclear centre is quite different from zero even in the energy domain $0\leq E\leq 10$ MeV, in which the absorptive potential $W(r;E)$ is entirely located at the nuclear surface. The fact that assumption (ii) is unjustified is illustrated by, e.g., Fig. 16 of Ref. 3, which shows that the dispersion relation (4.1) predicts a sizable central value $\Delta V(r=0;E)$ even at energies for which $W(r=0;E)\approx 0$; this is confirmed in Ref. 12. The explicit applications of the radial-dependent dispersion relation (4.1) made in Refs. 3 and 12 yield a dispersive contribution which is quite similar to that obtained in the framework of the present radial moment method; this confirms its reliability.

V. SUMMARY

The dispersion relation approach of Ref. 5 has been used to determine the energy dependence of the real part of the average n-^{89}Y potential. The inputs of the calculation are empirical values of the optical-model potential and of the single-particle energies. We choose the same input values as in Ref. 4 with two important differences, namely the following (Fig. 8): (i) We assume that the imaginary part of the potential is symmetric about the Fermi energy, in keeping with empirical as well as theoretical evidence; (ii) we include the effect of volume as well as of surface absorption.

We find that the modulus of the volume integral per nucleon of the real part of the average potential increases with energy in the close vicinity of the Fermi energy (Fig. 2), and that this is due to the increase of the potential radius (Fig. 3). At positive energy the modulus of the volume integral decreases with energy; this mainly reflects the decrease of the potential depth. The root mean square radius of the potential increases with energy in the vicinity of the Fermi energy, but decreases at small positive energy (Fig. 5). These features constitute the Fermi-surface anomaly.

In the dispersion relation approach the real part of the average potential is written as the sum of a Hartree-Fock–type component and of a dispersive contribution. The Hartree-Fock–type contribution is found to approximately have a Woods-Saxon radial shape with an energy-independent geometry and with a depth that decreases linearly with increasing energy (Fig. 2). The Fermi-surface anomaly is due to the dispersive contribution, which is surface-peaked near the Fermi energy but acquires a sizable central value already at small positive energy. The latter property is at variance with basic assumptions made in Ref. 4.

In conclusion, we have shown that the Fermi-surface anomaly is quite similar for the n-^{89}Y as for the n-^{208}Pb system. In both cases the anomaly is very difficult to detect from the analysis of neutron scattering data alone. Indeed, the volume integral of the average neutron-nucleus potential approximately has a linear energy dependence at positive energy, where the remnant anomaly reduces to a decrease of the potential root mean square radius with increasing energy. The anomaly becomes quite apparent when one simultaneously analyzes the bound single-particle energies and the scattering data; it consists of a characteristic modification of the energy dependence of both the volume integral and the root mean square radius as the neutron energy changes sign.

[1]G. E. Brown, J. H. Gunn, and P. Gould, Nucl. Phys. **46**, 598 (1963).
[2]G. F. Bertsch and T. T. S. Kuo, Nucl. Phys. **A112**, 204 (1968).
[3]C. Mahaux and H. Ngô, Nucl. Phys. **A378**, 205 (1982).
[4]R. D. Lawson, P. T. Guenther, and A. B. Smith, Phys. Rev. C **34**, 1599 (1986).
[5]C. Mahaux and R. Sartor, Phys. Rev. Lett. **57**, 3015 (1986).
[6]C. Mahaux and R. Sartor, Nucl. Phys. **A468**, 193 (1987).
[7]C. Mahaux and R. Sartor, Nucl. Phys. A (in press).
[8]C. Mahaux, P. F. Bortignon, R. A. Broglia, and C. H. Dasso, Phys. Rep. **120**, 1 (1985).
[9]C. Mahaux and R. Sartor, Nucl. Phys. **A460**, 466 (1986).
[10]R. L. Walter and P. P. Guss, in *Nuclear Data for Basic and Applied Science*, edited by P. G. Young, R. E. Brown, G. F. Auchampaugh, P. W. Lisowski, and L. Stewart (Gordon and Breach, New York, 1986), Vol. 2, p. 1079; P. G. Young, in Specialists' Meeting on the Use of the Optical Model for the Calculation of Neutron Cross Sections below 20 MeV, Report No. NEANDC-222U, OECD Nuclear Energy Agency, Paris, 1986, p. 127 (unpublished).
[11]G. E. Brown and M. Rho, Nucl. Phys. **A372**, 397 (1981).
[12]C. H. Johnson, D. J. Horen, and C. Mahaux, submitted to Phys. Rev. C.
[13]C. Mahaux and R. Sartor, Phys. Rev. C **34**, 2119 (1986).
[14]R. D. Lawson, P. T. Guenther, and A. B. Smith, Argonne National Laboratory report, 1987.